Hybrid Fuel Cell-Battery-Supercapacitor Energy Management System controlled by sliding modes

Héctor Gerardo Chiacchiarini
Dpto. de Ing. Eléctrica y de Computadoras,
Universidad Nacional del Sur (UNS),
Instituto de Inv. en Ing. Eléctrica "Alfredo Desages" (IIIE), Universidad Nacional del Sur (UNS) - CONICET,
Bahía Blanca, Argentina.
E-mail: hgch@uns.edu.ar

Ezequiel Orozco
Dpto. de Ing. Eléctrica y de Computadoras,
Universidad Nacional del Sur (UNS),
Bahía Blanca, Argentina.
E-mail: ezequieloro9@gmail.com

***Abstract*— Hybrid Energy Storage Systems composed by more than a single energy source and/or energy storage devices can show better performance than single devices when an adequate Energy Manager System is designed. A sliding mode control is used in this paper for an energy management system of a hybrid energy source and storage system composed by a hydrogen fuel cell, a battery and a supercapacitor. The manager splits the power demand of an electric traction system over the energy source and the two storage devices, preventing the battery and the fuel cell to be stressed by fast changing current demands, thus preserving their lifespan, while responding adequately to the traction system current demand. Simulation results show adequate performance.**

Keywords*— *Energy management; Energy storage; Sliding mode control; Fuel Cell;, Supercapacitor; Battery; Electric traction.

I. INTRODUCTION

Lithium-Ion (Li-ion) batteries (B) technologies offer high performance devices [1] with increasing energy density. Actually, they are still costly devices suffering from degradation problems under normal usage [2] that have to be properly addressed to preserve B health [3], [4]. Batteries and other storage devices (e.g B, Fuel Cell (FC) and Supercapacitors (SC), or B and SC) can be combined to create Hybrid Energy Storage System (HESS) where the advantages of each device can be exploited in a proper way [5], [6]. Such HESS need an Energy Management System (EMS) to coordinate the usage of each device while preserving its global health [7]. Excessive stress on the B may lead to overheating and premature degradation, among other effects. The B health depends on the current demand, cycling, temperatures, and other factors. Fast changing current demands on the FC will affect negatively its instantaneous voltage level and will stress its auxiliary mechanisms. This work presents an EMS based on sliding mode control for a hybrid combination of FC, B and SC which splits the power demand over the three devices while preventing the B and FC to be overstressed by fast-changing current demands.

Sliding Modes (SM) are particular dynamic responses obtained on systems with variable structure [8]. A well-known property of Sliding Mode Control (SMC) is the capacity of sustain an invariant closed loop dynamics against certain kind of parametric perturbations and exogenous signals. Also, simplicity of design and implementation are appreciated advantages respect to other alternatives. A SMC strategy for the EMS of a HESS is presented by [9] using classical linear sliding surface to control the B and SC currents to their reference values. Also a SMC is developed by [10] to drive the SC and B currents to their reference values using also estimators to obtain the load current and external voltages. Again, a classical linear sliding surface is used. In particular, some authors have focused on the design of EMS for HESS using SMC but there are not many cases where nonlinear sliding surfaces are used.

Boost converters show non-minimum phase behavior considering the output voltage respect to the control input. Thus, the selection of a sliding surface just involving the output voltage error will impose an unstable dynamics on the inductor current. Some control options are: Indirect control imposing a prescribed behavior on the inductor current such that the output voltage can be regulated, or taking advantage of the differential flatness property when choosing as output the total energy stored in the system [11]. The SM control strategy used here explores the use of a nonlinear sliding surface evaluated from the total energy stored in the devices. It seeks for dynamic decoupling between the current waveform provided by the SC and the current waveforms provided by the B and FC, while at the same time regulating the SC SoC, the B SoC, and the dc-link voltage. The proposed control structure is composed by three independent sliding controllers: One designed to command the SC current to satisfy the load demand while regulating the dc-link voltage; other one oriented to regulate the SC SoC; and the third to restore the B SoC. This work extends preliminary results presented in [12] where a simpler B-SC HESS was studied, and previous results presented in [13] for a FC-B-SC system with a different recharging strategy. The sliding dynamics is designed such that the SC can react to fast current changes, while the other devices can provide an average power demand needed to restore the SC State of Charge (SoC) and also the B SoC. The system is an active parallel architecture.

The objective here is to evaluate the feasibility and complexity of this control strategy, explore the advantages and

detect possible disadvantages related to the effective use of this EMS for HESS. The work is organized as follows: The system architecture and SMC strategy are presented below, followed by simulation results. The last section presents some conclusions and recommendations about perspectives for future work.

II. SYSTEM ARCHITECTURE

Fig. 1 shows the HESS composed by an H_2 FC, B and a SC, all connected to a capacitive dc bus by bidirectional boost-Buck converters, and where a bidirectional full bridge converter fed from the dc bus drives the traction motor. The load current and the currents provided by the storage and source devices are driven by switched PWM converters operated at high frequency and in general will have discontinuous pulsed behavior. This produces a high frequency ripple on the voltage of the dc-link capacitor and on the inductance currents, which usually cannot be compensated by the control loop. Then, as for control purposes it is adequate to get rid of this ripple effect, the averaged variations of the dc-link voltage and inductance currents are evaluated using the input-output power balance equations on the converters. Also, measurements are low-pass filtered. So, it is considered an averaged dynamic model as:

$$C_{dc}\,\dot{V}_{dc} = u_b I_{L_b} + u_{sc} I_{L_{sc}} + u_{fc} I_{L_f} - I_0, \quad (1)$$

$$L_b \dot{I}_{L_b} = V_b - V_{dc} u_b, \quad (2)$$

$$L_{sc} \dot{I}_{L_{sc}} = V_{sc} - V_{dc} u_{sc}, \quad (3)$$

$$L_{fc} \dot{I}_{L_f} = V_{fc} - V_{dc} u_{fc}, \quad (4)$$

$$\dot{V}_b = f\left(I_{L_b}\right), \quad (5)$$

$$C_{sc} \dot{V}_{sc} = -I_{L_{sc}}, \quad (6)$$

$$V_{fc} = V_{fc0} - R_{fc} I_{L_f}, \quad (7)$$

where the electric variables (shown in Fig. 1) represent the average behavior of the instantaneous voltages and currents, and the control signals u_b, u_{fc}, u_{sc} are the duty cycles (d.c) of the PWM drivers. Parameter R_{fc} in (7) represents the ohmic behavior of the FC for the output current range between the activation current and the point of maximum output power. Function $f(\cdot)$ in (5) has to be adjusted according to the B chemistry and configuration. As a first approximation, for control purposes it can be approximated by a capacitive behavior similar to (6), considering an equivalent capacitance that creates a voltage variation of similar magnitude as the B voltage variation when its charge changes from $SoC = 0$ to $SoC = 100\%$.

III. SMC STRATEGY

The objective is to indirectly regulate the dc-link voltage V_{dc} at a specific set point, by using the energy stored in the SC. For that, an adaptation of a standard procedure for the boost converter control in sliding mode is used, as will be explained below. Simultaneously the SC energy is restored from the B and from the FC using other sliding controllers to regulate their currents according to a slowly varying reference signal.

A. Regulator design

The first control loop will include the SC and the dc-link. The total averaged energy stored in the dc-link and the inductances of the SC, FC and B converters is

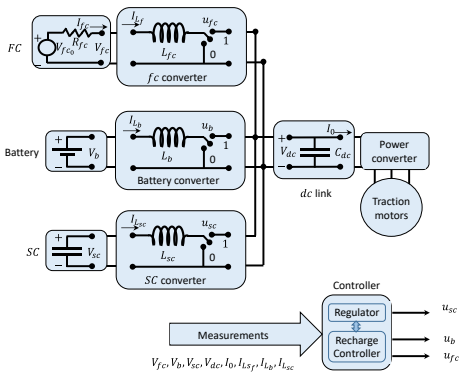

Fig. 1 Schematic diagram of the EMS.

$$E_0 = \frac{1}{2} C_{dc} V_{dc}^2 + \frac{1}{2} L_{sc} I_{L_{sc}}^2 + \frac{1}{2} L_b I_{L_b}^2 + \frac{1}{2} L_{fc} I_{L_f}^2. \quad (8)$$

As I_0 is usually varying due to the load demand, and the B and FC currents are restricted to have slow variations, the reference energy has to include the SC current, as follows

$$E_0^*(t) := \frac{1}{2} C_{dc} \bar{V}_{dc}^2 + \frac{1}{2} L_b \bar{I}_{Lb}^2 + \frac{1}{2} L_{fc} \bar{I}_{Lf}^2 + \frac{1}{2} L_{sc} \left(\frac{\bar{V}_{dc}}{V_{sc}} I_0 - \frac{V_b}{V_{sc}} \bar{I}_{Lb} - \frac{V_{fc}}{V_{sc}} \bar{I}_{Lf} \right)^2, \quad (9)$$

where $\bar{I}_{Lb}, \bar{I}_{Lf}$ are created by the SC voltage controller.

That allows the definition of the energy error output

$$e := E_0 - E_0^*(t), \quad (10)$$

which has to be driven to zero by the closed loop controller. Using (8), (9), and later using (1), …, (4):

$$\dot{e} = \Sigma := I_{L_{sc}} V_{sc} + I_{L_b} V_b + I_{L_f} V_{fc} - V_{dc} I_0 - \dot{E}_0^*(t), \quad (11)$$

where, after neglecting the effects of $\dot{\bar{V}}_{dc}$, $\dot{V}_b, \dot{V}_{fc}$ and $\dot{V}_{sc}$,

$$\dot{E}_0^*(t) = L_b \bar{I}_b \dot{\bar{I}}_b + L_{fc} \bar{I}_{Lf} \dot{\bar{I}}_{Lf} + L_{sc} \left(\frac{\bar{V}_{dc}}{V_{sc}} I_0 - \frac{V_b}{V_{sc}} \bar{I}_b - \frac{V_{fc}}{V_{sc}} \bar{I}_{Lf} \right) \left(\frac{\bar{V}_{dc}}{V_{sc}} \dot{I}_0 - \frac{V_b}{V_{sc}} \dot{\bar{I}}_b - \frac{V_{fc}}{V_{sc}} \dot{\bar{I}}_{Lf} \right). \quad (12)$$

This shows that the derivative of the energy error is dependent on the instantaneous input-output power balance, and does not depend on the control inputs, thus the relative degree (r.d.) of e is higher than one. Evaluating now

$$\ddot{e} = \dot{I}_{L_{sc}} V_{sc} + \dot{I}_{L_b} V_b + \dot{I}_{L_f} V_{fc} - \dot{V}_{dc} I_0 + I_{L_{sc}} \dot{V}_{sc} + I_{L_b} \dot{V}_b + I_{L_f} \dot{V}_{fc} - V_{dc} \dot{I}_0 - \ddot{E}_0^*(t), \quad (13)$$

and using also (5), (6), (7), considering $\dot{V}_{fc0} = 0$:

$$\ddot{e} = A_1 - u_{fc} B_3 - u_b B_2 - u_{sc} B_1, \quad (14)$$

where $A_1 := \frac{V_{sc}^2}{L_{sc}} + \frac{V_b^2}{L_b} + \frac{V_{fc}^2}{L_{fc}} - \frac{I_{L_f} R_{fc} V_{fc}}{L_{fc}} - \frac{I_{Lsc}^2}{C_{sc}} + I_{L_b} f\left(I_{L_b}\right) + \frac{I_0^2}{C_{dc}} - V_{dc} \dot{I}_0 - \ddot{E}_0^*(t)$, $B_1 := \left(\frac{V_{sc} V_{dc}}{L_{sc}} + \frac{I_{Lsc} I_0}{C_{dc}} \right)$, $B_2 := \left(\frac{V_b V_{dc}}{L_b} + \frac{I_{Lb} I_0}{C_{dc}} \right)$, $B_3 := \left(\frac{\left(V_{fc} - I_{L_f} R_{fc}\right) V_{dc}}{L_{fc}} + \frac{I_{Lf} I_0}{C_{dc}} \right)$, and considering

negligible the effects of $\dddot{\bar{V}}_{dc}$, $\dot{V}_b$ and $\dot{V}_{sc}$, $\ddot{E}_0^*(t) = L_{sc}\left(\frac{\bar{V}_{dc}}{V_{sc}}\dot{I}_0 - \frac{V_b}{V_{sc}}\dot{\bar{I}}_b - \frac{V_{fc}}{V_{sc}}\dot{\bar{I}}_{Lf}\right)^2 + L_{sc}\left(\frac{\bar{V}_{dc}}{V_{sc}}I_0 - \frac{V_b}{V_{sc}}\bar{I}_b - \frac{V_{fc}}{V_{sc}}\bar{I}_{Lf}\right)\left(\frac{\bar{V}_{dc}}{V_{sc}}\ddot{I}_0 - \frac{V_b}{V_{sc}}\ddot{\bar{I}}_b - \frac{V_{fc}}{V_{sc}}\ddot{\bar{I}}_{Lf}\right) + L_b\dot{\bar{I}}^2{}_b + L_b\bar{I}_b\ddot{\bar{I}}_b + L_{fc}\dot{\bar{I}}^2{}_{Lf} + L_{fc}\ddot{\bar{I}}_{Lf}\bar{I}_{Lf}$.

It is verified that $\ddot{e}$ is linearly dependent on the control signals u_{sc}, u_b, u_{fc} if $B_1 \neq 0$, $B_2 \neq 0$, $B_3 \neq 0$ respectively, having e r.d. 2 respect to each control signals whenever those conditions are satisfied. The particular possible situation of losing the r.d. condition respect to u_{sc} is only found for voltages and currents outside of the operational range. The special cases $B_2 = 0$ or $B_3 = 0$ just make (14) independent of the respective control signals u_b or u_{fc}. The special case $B_1 = 0$, if happens, will make u_{sc} to saturate towards 0 or 1 (see (18) below), thus forcing $I_{L_{sc}}$ to increase or decrease until $B_1 \neq 0$ again.

The main objective is to regulate the voltage V_{dc} which is affected by the load current I_0. By design, the system must guarantee that the SC current I_{Lsc} can react fast enough to compensate the effects of the variations of I_0.

To drive the energy error $e \to 0$, it is proposed to force the following reduced order dynamics

$$\dot{e} = -ke, \tag{15}$$

where $k > 0$ is selected according to the desired convergence speed. For that, a SMC is proposed to drive the signal $\sigma_0 := ke + \dot{e} \to 0$ in finite time by manipulating u_{sc}, while considering that u_b, u_{fc} are known perturbations manipulated by other controllers designed to regulate the SC voltage and to recharge the B. So, the r.d. condition assures the dependence of the time derivative $\dot{\sigma}_0$ on the control variables as shown below:

$$\dot{\sigma}_0 = k\dot{e} + \ddot{e} = \alpha - B_1 u_{sc}\,, \tag{16}$$

where $\alpha := \phi - u_b B_2 - u_{fc}B_3$, and $\phi := k\Sigma + A_1$.

The equivalent control $u_{sc_{eq}}$ [8] is obtained by solving $\dot{\sigma}_0 = 0$ assuming for the sequel $B_1 \neq 0$, as $u_{sc_{eq}} := \alpha/B_1$ and the sliding mode will be possible if and only if $0 \leq u_{sc_{eq}} \leq 1$. The reaching condition is

$$\frac{\sigma_0}{|\sigma_0|}\dot{\sigma}_0 \leq -\eta, \eta > 0. \tag{17}$$

Using (16) and considering the equality in (17), the d.c. of the SC converter is obtained as

$$u_{sc} := \mathrm{Sat}_0^1\left\{\frac{\alpha}{B_1} + \frac{\eta}{B_1}Sign(\sigma_0)\right\}, \tag{18}$$

where $Sat_a^b\{x\} := b(\,x > b) + x(a \leq x \leq b) + a(\,x < \mathrm{a})$. The following section describes the controllers for u_b and u_{fc}.

B. Recharge Controller design

Regarding the FC as the main energy source, the B as an auxiliary storage device and the SC as responsible of providing the instantaneous power to balance the dc-link voltage, many strategies can be created to recharge the SC, keep the B SoC within a desired range and operate the FC according to its capacity limitations and best practices. Due to the faster reaction of the SC controller, the average power injected to the dc link by the B and FC converters will be compensated by an equivalent power extracted from there by the SC converter, thus forcing a recharge current into the SC. From (1), and considering that the FC and B operation dynamics is planned to be much slower than the SC´s, the FC and B converters can be assumed to operate at steady state considering their input-output averaged power balance. So, the current balance at the dc link can be stated as

$$C_{dc}\,\dot{V}_{dc} = \frac{V_b}{V_{dc}}I_{L_b} + u_{sc}I_{L_{sc}} + \frac{V_{fc}}{V_{dc}}I_{L_f} - I_0. \tag{19}$$

The current references for the B and FC converters will be created to slowly restore the averaged SC and B SoC.

The restoration dynamics is designed to be slow with respect to the dc link closed loop dynamics, and compatible with the B and FC best usage practices. It is proposed to command the FC and B converters to feed coordinately into the dc-link an averaged current $\bar{I}_{r0}$ to recharge the B and SC. Ideally,

$$\bar{I}_{r0} := \bar{I}_{rsc0}, \tag{20}$$

where signal $\bar{I}_{rsc0}$ stands tor the necessary average recharging current feeding the dc link to restore the SC SoC.

As the battery will also need recharging, (20) is rewritten to include the B recharge current as

$$\bar{I}_{r0} := \bar{I}_{rsc0} + \bar{I}_{rb0} - \bar{I}_{rb0}, \tag{21}$$

where signal $\bar{I}_{rb0}$ stands for the necessary average recharging current feeding the dc link to restore the B SoC. Clearly it is equivalent to (20) but after explicitly including $\bar{I}_{rb0}$ the B recharge strategy will become more clear in next paragraphs.

Signal $\bar{I}_{r0}$ is further split in two additive components, $\bar{I}_{Lf0}$ and $\bar{I}_{Lb0}$ following some adequate criteria. A specific one will be described below. Other one can be found in [13]. Component $\bar{I}_{Lf0}$ is the averaged desired output current of the FC converter (commanded to set I_{Lf} as FC current). Component $\bar{I}_{Lb0}$ is the averaged desired output current of the B converter (commanded to set I_{Lb} as B current). Both defined to satisfy

$$\bar{I}_{Lf0} + \bar{I}_{Lb0} = \bar{I}_{r0}, \tag{22}$$

playing each one the role of collecting one or more terms of the right member of (21). So, the ideal converter controller references should be $\bar{I}_{Lb} = \frac{V_{dc_{av}}}{V_{b_{av}}}\bar{I}_{Lb0}$, $\bar{I}_{Lf} = \frac{V_{dc_{av}}}{V_{fc_{av}}}\bar{I}_{Lf0}$. The averaged quantities $V_{dc_{av}}, V_{b_{av}}, V_{fc_{av}}$ are obtained by low-pass filtering the measured values. Filters bandwidth is set to cutoff the undesired high-frequency components, shaping slowly varying waveforms.

The operative range of the FC restricts $I_{Lf} \in \left[I_{Lf_m}, I_{Lf_M}\right]$, where I_{Lf_m} is the minimum activation current, and I_{Lf_M} is the current where the maximum power is drained. Also the B operative range is restricted to $I_{Lb} \in \left[-I_{Lb_{ch}}, I_{Lb_{dis}}\right]$, where $I_{Lb_{ch}}$ represents the maximum allowed charging current, and $I_{Lb_{dis}}$ is the maximum allowed discharge current. Those limit values are dependent on the actual B SoC, State of Health (SoH) and temperature. The designer has to define them according to the B condition.

An adequate criterion has to be defined to create both current references, and several options arise for this combination of FC

and B. The simplest option, but probably not the best, is to assign to the B the role of recharging the SC while keeping inactive the FC until it is necessary to recharge the B. This scenario forces charge cycling on the B and on-off cycling of the FC, incrementing power losses due to the energy flow through the converters and through the B output impedance. Although not the best, this criterion was adopted in [13] to complete a basic design.

Here, a different strategy commands the FC to provide the averaged power necessary for the traction and recharge systems. The SC is commanded to react to the instantaneous demands of the system, while the FC and battery are commanded to provide the average current demanded by the load and for SC recharging. Battery recharging task is assigned to the FC.

Due to the faster reaction of the SC controller, the average power injected by the FC converter to the dc link will be compensated by an equivalent and opposite value of power extracted from there by the SC converter, thus forcing a recharge current into the SC. Simultaneously, the battery converter current is defined to complement the slow reaction of the FC and simultaneously drain the assigned recharge current, while adopting the battery best usage practices.

The FC, as the main energy provider, is commanded to surge the low frequency components of the averaged load demand and averaged recharge needs for the battery and SC. The battery is commanded to complement the FC providing some higher frequency components, and accepting the recharge energy.

To start, signals $\bar{I}_{rb}$, $\bar{I}_{rsc}$ and $\bar{I}_{0av}$ need to be defined:

Signal $\bar{I}_{rb}$ stands for the necessary recharge current to recover the battery SoC, defined here as follows:

$$\bar{I}_{rb} := \begin{cases} I_{Lb_{dis}} & if \quad \overline{SoC} \le SoC_b, \\ I_{Lb_{dis}}\left(\frac{SoC_b - SoC_M}{\overline{SoC} - SoC_M}\right) & if \quad SoC_M < SoC_b < \overline{SoC}, \\ 0 & if \quad SoC_b \in [SoC_m, SoC_M], \\ -I_{Lb_{ch}}\left(\frac{SoC_m - SoC_b}{SoC_m - \underline{SoC}}\right) & if \quad \underline{SoC} < SoC_b < SoC_m, \\ -I_{Lb_{ch}} & if \quad SoC_b \le \underline{SoC}. \end{cases} \tag{23}$$

$$\bar{I}_{rb0} = \frac{V_{b_{av}}}{V_{dc_{av}}}\bar{I}_{rb} \tag{24}$$

Variables $\overline{SoC} > SoC_M > SoC_m > \underline{SoC}$, are all adequately defined in the range 0 to 100% to set the recharging strategy of the battery.

Signal $\bar{I}_{rsc}$ stands tor the necessary recharging current to restore the SC SoC, usually adequately defined as a function of the SC SoC or voltage, and defined here as follows:

$$\bar{I}_{rsc} := \gamma\left(\bar{V}_{sc} - V_{sc_{av}}\right) + I_{Lsc_{av}}, \tag{25}$$

$$\bar{I}_{rsc0} = \frac{V_{sc_{av}}}{V_{dc_{av}}}\bar{I}_{rsc}$$

where gain $\gamma > 0$ is defined according to the desired recharging dynamics for the SC.

Signal $\bar{I}_{0av} := LP_3(I_0)$ is obtained by low-pass filtering the load current I_0 with an adequately designed third order filter, to allow smooth enough variations at start-up under step changes of I_0.

Now, from (21), (22) the following recharge current distribution is chosen:

$$\bar{I}_{Lf0} = \bar{I}_{rsc0} - \bar{I}_{rb0},$$
$$\bar{I}_{Lb0} = \bar{I}_{rb0}.$$

But, for the FC to source the recharging current for the battery and to provide the average current load to the traction inverter, the FC converter should be ideally commanded by

$$\bar{\bar{I}}_{Lf} = \frac{V_{dc_{av}}}{V_{fc_{av}}}\bar{I}_{LfT0},$$
$$I_{LfT0} := \bar{I}_{Lf0} + \bar{I}_{oav}.$$

Note that the addition of $\bar{I}_{oav}$ above is a feedforward action that helps to push $I_{Lsc_{av}}$ towards zero since the only power source is the FC, while B and SC just operate to adjust transient behaviors.

For the battery to source the recharging current for the SC while restoring its SoC, the battery converter should be ideally commanded by

$$\bar{\bar{I}}_{Lb} = \frac{V_{dc_{av}}}{V_{b_{av}}}\bar{I}_{Lb0}.$$

Due to natural limitations of the FC performance and current, and due to current limitations of the battery, the references are modified as follows

$$\bar{I}_{Lf} := LP_3\left(Sat_{I_{LF_m}}^{I_{Lf_M}}\left(\bar{\bar{I}}_{Lf}\right)\right), \tag{26}$$

$$\bar{I}_{Lb} := LP_2\left(Sat_{-I_{b_{ch}}}^{+I_{b_{dis}}}\left(\frac{V_{dc_{av}}}{V_{b_{av}}}\left(\bar{I}_{LfT0} - \frac{V_{fc_{av}}}{V_{dc_{av}}}\bar{I}_{Lf}\right) + \bar{\bar{I}}_{Lb}\right)\right), \tag{27}$$

which correspond to the required contribution of the B and FC to $\bar{I}_{r0}$ (21) and to the traction inverter according to the its capabilities and to its recharging needs. Operator $LP_3(\cdot)$ is a third-order low pass filter with critical damping response, designed to shape the $\bar{I}_{Lf}$ waveform and $LP_2(\cdot)$ is a second order low-pass filter designed for similar purpose. The bandwidth of filter $LP_2(\cdot)$ is set to be wider than the bandwidth of $LP_3(\cdot)$ but its cutoff frequency should be selected to filter out undesired high-frequency components that could affect somehow the battery. As seen above, the battery also is commanded to supply the current that the FC cannot provide due to its dynamic limitations.

Jointly, due to their dynamic limitations, the FC and battery usually are not able to provide exactly the demand $\bar{I}_{r0} + \bar{I}_{oav}\ \forall t$, so the SC has to complement the charge flow during transients.

■

Once $\bar{I}_{Lb}$ and $\bar{I}_{Lf}$ are defined, local controllers for each converter have to force $e_b = I_{Lb} - \bar{I}_{Lb} \to 0$ and $e_{fc} = I_{Lf} - \bar{I}_{Lf} \to 0$. Again, simple SMC are designed as shown below.

For the B controller: Let $\sigma_b = e_b$ be the desired sliding output. It is verified that σ_b has r.d. 1 since using (2) $\dot{e}_b = \dot{I}_{Lb} - \dot{\bar{I}}_{Lb} = \frac{V_b - V_{dc}u_b}{L_b} - \dot{\bar{I}}_{Lb}$, which is linearly dependent on u_b.

The reaching condition is defined as

$$\frac{\sigma_b}{|\sigma_b|}\dot{\sigma}_b \leq -\eta_b, \eta_b > 0, \qquad (28)$$

being η_b the minimum variation speed imposed to $\dot{\sigma}_b$.

Now, replacing $\dot{\sigma}_b$ and considering the equality, it leads to the d.c. of the B converter defined by

$$u_b := \mathrm{Sat}_0^1\left\{\frac{V_b}{V_{dc}} - \frac{L_b}{V_{dc}}\dot{\bar{I}}_{Lb} + \frac{L_b}{V_{dc}}\eta_b Sign(\sigma_b)\right\}. \qquad (29)$$

The signal $\bar{I}_{Lb}$ is assumed to be slowly varying so its time derivative $\dot{\bar{I}}_{Lb}$ can be neglected in the control loop, or eventually evaluated with an adequate differentiator filter.

Following an equivalent procedure, for $\sigma_{fc} = e_{fc}$, using (4) and for an adequate value of η_{fc}, the d.c. of the FC controller is

$$u_{fc} := \mathrm{Sat}_0^1\left\{\frac{V_{fc}}{V_{dc}} - \frac{L_{fc}}{V_{dc}}\dot{\bar{I}}_{fc} + \frac{L_{fc}}{V_{dc}}\eta_{fc} Sign(\sigma_{fc})\right\}. \qquad (30)$$

The signal $\bar{I}_{Lf}$ is also assumed to be slowly varying so its time derivative $\dot{\bar{I}}_{Lf}$ can be neglected in the control loop, or evaluated with an adequate differentiator filter.

IV. Results

The performance of the proposed strategy was analyzed with simulations. In the future may be possible to perform experiments. A standard simulation software was used, implementing a fixed step integration algorithm with a maximum time step size of 2 μs. The simulation was run for one second to let the system to stabilize at an (almost) steady state condition. All that initial data was discarded, the timer is reset to zero and the figures show the evolution after that time up to 100 more seconds. The used SC dynamic model is a commonly used one, following [14], [15]. The B dynamic model also is a standard one, following [16]. The FC model follows [17], [18] and its electrical characteristic is depicted in Fig. 2 where the nominal operating point $[15A, 48V]$ and maximum operating point $[20A, 46V]$ are depicted. The converters were simulated by their averaged behavior, discarding ripple effects and averaging discontinuous pulsating currents. The converter switches were simulated as a function of the d.c. using their averaged effect on the circuits. The simulated system parameters are listed in Table I. The case study considers the initial condition of the system in steady state: The output current $I_0 = 0$, the SC loaded at its reference voltage and the B SoC slightly less than 25%. So no recharge current is needed from the B for the SC, but the B is needing recharge from the FC.

After one second a sudden request of $I_0 = 8A$ is imposed during a whole second and then changed to $-2A$ for 0.25 s. After that, a pulsed current demand of $+8A, -2A$, of period 0.5s and 50% d.c. is sustained. This waveform is chosen to illustrate the capabilities of the design. The selected current demand shows an average positive demand current of $3A$ with an additive pulsed demand of $\pm 5A$, useful to show the long term response and the short term transient behavior.

TABLE I. Main System Parameters

Parameter	Value	Parameter	Value
C_{sc}	160 $[F]$	Battery capacity	10 $[Ah]$
L_{sc}	800 $[\mu Hy]$	Nominal battery voltage	48 $[V]$
L_b	800 $[\mu Hy]$	FC maximum power	920 $[W]$
L_{fc}	800 $[\mu Hy]$	FC maximum output current	20 $[A]$
C_{dc}	2400 $[\mu F]$	FC maximum output voltage	65 $[V]$
$\lvert I_{Lb}\rvert$	≤ 10 $[A]$	FC maximum efficiency current	15 $[A]$

The recharge demand for the battery $\bar{I}_{rb}$ (23) is shown in Fig. 3 where $\overline{SoC} = 90\%, SoC_M = 75\%, SoC_m = 35\%$, $\underline{SoC} = 20\%$. Fig. 4.(a) shows the averaged load current drained by the traction converter, and the dc link voltage V_{dc}, which is initially at $V_{dc} = 75V$ and later becomes barely affected by the current load. The voltage ripple is affected by the use of a simplified model for the SC and B for the control design, where their internal resistances are neglected. It is also worth to mention that such voltage ripple does not affect the traction performance since the traction inverter controller is able to compensate it. In this case it shows less ripple compared to [13]. Fig. 4.(b) shows the averaged output current at the SC terminals $I_{L_{sc}}$ which is equal to the current flowing through the respective SC converter inductor L_{sc}. It shows less low frequency variations compared to [13]. Fig. 4.(c) shows the averaged output current at the B terminals I_{L_b} and flowing through the corresponding converter inductor L_b. Fig. 4.(d) shows the averaged output current at the FC terminals I_{L_f} and flowing through the corresponding converter inductor L_{fc}. The results included in [13] shown that I_{Lf} is almost constant while I_{L_b} is providing all necessary fluctuations, but here the effort is shared between FC and B. Both I_{Lf} and I_{Lb} react slowly creating a current flow to the dc-link forcing the regulator to adjust the SC current. So, a net current flow appears from the B to the SC when it needs recharging, and vice versa. Also, the FC recharges the B when

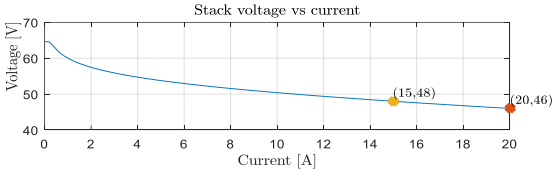

Fig. 2 FC Polarization curve.

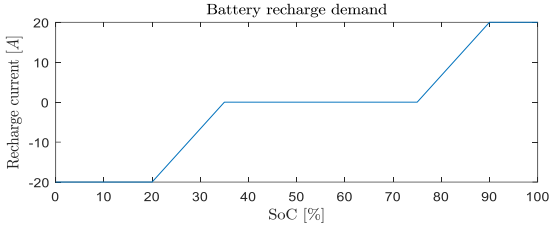

Fig. 3 Recharge demand for the battery as a function of its SoC.

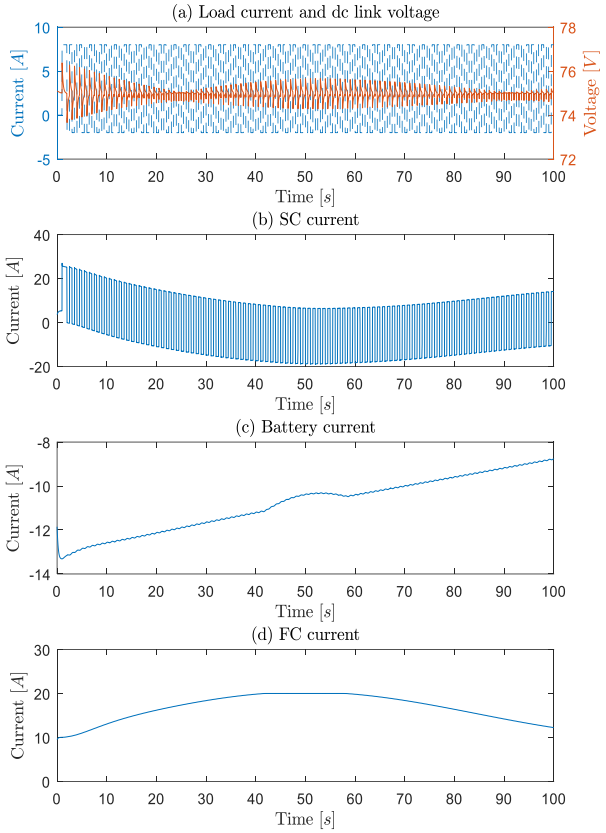

Fig. 4 (a) Averaged current demand I_0 produced by the traction power converter and averaged dc-link voltage V_{dc}; (b) Averaged output current at the SC terminals $I_{L_{sc}}$; (c) Averaged output current at the battery terminals I_{L_b}, (d) Averaged output current at the FC terminals I_{fc}.

needed. The smooth variation of the currents preserve both devices from the effects of high-frequency currents.

For the case study, $\gamma = 50$ in (25), operator LP_3 in (26) has a triple pole at $\omega_n = 2\pi\ [1/s]$ and operator LP_2 in (27) has a double real pole at $2\omega_n$.

It is worth to mention that the sliding regulator operates on the global energy error (10) as shown in Fig. 5, instead of on the voltage error. The shown error is less than 3% of the stored energy. During sliding mode, the energy error e evolves following the dynamics (15) given by $\dot{e} = -k.e$, where for the case it was selected $k = 5\ [1/s]$.

Fig 6 shows the sliding outputs σ_0, σ_b and σ_{fc}. It is seen that σ_0 is barely affected by the sudden load changes, while σ_b and σ_{fc} remain practically around zero the whole time. The spikes on σ_0 are mainly due to the finite time step of the simulation and the first-order derivative filters used to evaluate $\dot{I}_0, \ddot{I}_0$. The same effect is seen on σ_b, but with negligible amplitude. Note the fast reaching phases towards zero. The evolution of these signals is similar as in [13].

Fig. 7.(a) shows the evolution of the SC voltage V_{sc} and its SoC, due to the effects of the drained current. Please note the effect of the internal SC output resistance on V_{sc} due to the current I_{sc}, producing step changes on the voltage. In addition, Fig 7.(b) shows the same for the B. The shown voltage decreases

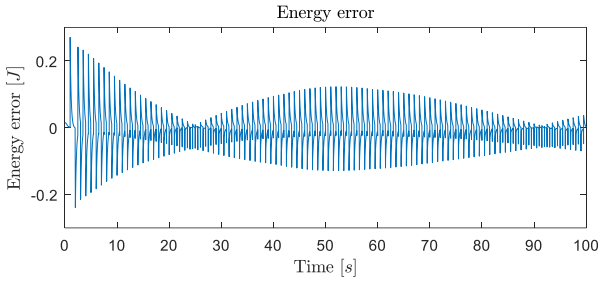

Fig. 5 Difference between the total stored energy at the inductances and dc-link capacitor, and the reference energy value.

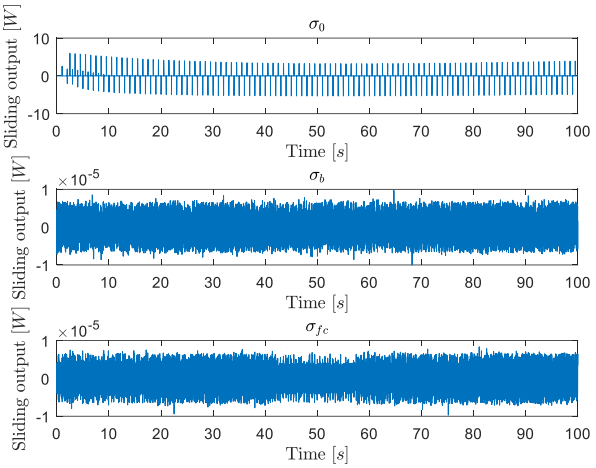

Fig. 6 Sliding output σ_0 used by the sliding regulator (above). Sliding outputs σ_b, σ_{fc} used by the sliding recharge controllers (center and below).

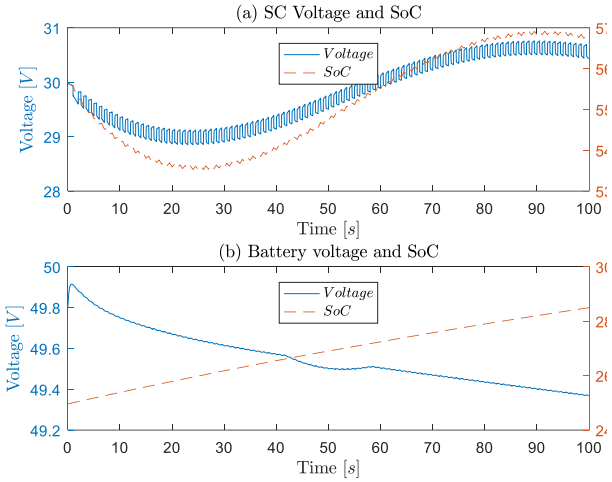

Fig. 7 (a) Evolution of the SC voltage V_{sc} and its State of Charge (SoC); (b) Evolution of the battery voltage V_b and its State of Charge (SoC).

continuously while the SoC increases, due to the effect of the variable recharge current on the B output resistance, as shown in Fig. 4.(c). The d.c. u_b, u_{sc}, u_{fc} are presented in Fig. 8 where the discontinuous behavior of the sliding controller is easily noted. The discontinuous gains were selected as $\eta_b = \eta_{fc} = 30, \eta_0 = 100$. Sudden reactions occur when the sliding variables σ_0, σ_b, σ_{fc} jump away from zero due to step changes in the current demand.

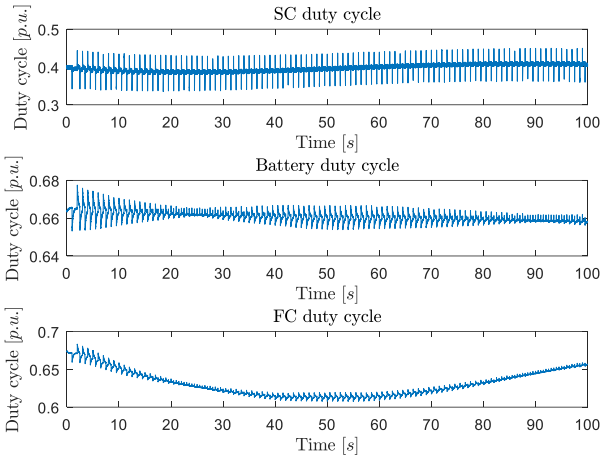

Fig. 8 Duty cycle of the SC PWM driver (above). Duty cycle of the battery PWM driver (center). Duty cycle of the FC PWM driver (below).

V. CONCLUSIONS

A sliding mode control strategy was used to implement an EMS on a hybrid FC-B-SC HESS. The SC is commanded to provide the fast response while the B is used to slowly adjust the SC charge. The FC is used to restore the B SoC. The performance can be adjusted independently defining the desired time response of the charge restoring of the dc-link capacitor, the SC, and the B. The B health is preserved by limiting high frequency components of the B current. Other health preservation actions could also be considered, as for example: preventing extreme state of charge conditions, preventing extreme temperatures, and limiting the charge-discharge cycles. The proposed control strategy can be extended to include other restrictions according to the needs. E.g., it is simple to add a charge-discharge oscillatory behavior between B and SC to heat up the B if necessary, as presented in [4].

The sliding mode strategy in general provides robustness to the control loop, and invariance against matched perturbations. Although some equations seem complex to evaluate, the control strategy follows rather simple ideas, being also possible to simplify some expressions at a cost of increasing the switching gains $\eta_0, \eta_b, \eta_{fc}$, preserving a satisfactory performance. It is worth to highlight the design simplicity and adjustment of the controller tuning parameters to obtain a desired closed loop performance. The design of expressions (23), (25), (26), (27) condition the charge/discharge cycles of the B and the FC operative conditions. Its design has to be done considering the SC capacity and the maximum load current, which together define the SC charge/discharge time. Naturally, the expected reaction speed of the recharge control loop must be high enough to guarantee proper regulation of the SC SoC, but an excessive reaction speed would increase the B cycling thus degrading the lifespan. The results presented here show better behaviour compared to [13]: The dc link voltage ripple is lower; current $I_{L_{sc}}$ shows less low frequency variations; and the recharge effort is shared smoothly between the FC and B.

Considering future possible actions to continue this ideas, experiments will be necessary to highlight possible practical issues regarding the implementation, and to confirm its advantages in practice.

ACKNOWLEDGMENT

The authors thank the support of Universidad Nacional de Sur and CONICET.

REFERENCES

[1] Opitza, A., P. Badamia, L. Shena, K. Vignaroobana, A.M. Kannana, “Can Li-Ion batteries be the panacea for automotive applications?”, Renewable Sustainable Energy Rev. 68 (2017) 685–692.

[2] Wang, X., Kerr, R., Chen, F., Goujon, N., Pringle, J.M., Mecerreyes, D., Forsyth, M., Howlett, P.C., Toward high-energy-density lithium metal batteries: opportunities and challenges for solid organic electrolytes, Advanced Materials, 32 (18), art. no. 1905219, 2020.

[3] Kabir, M., D. Demirocak, “Degradation mechanisms in Li-ion batteries: a state-ofthe-art review”, Int. J. Energy Res. 2017; 41:1963–1986.

[4] Chiacchiarini, H., C. De Angelo, G. Amaya, Health-conscious energy management of a hybrid battery-supercapacitor storage system, 27° Cong. Argentino de Control Automático, Buenos Aires, Arg. Oct. 2020.

[5] Amaya, E. G., H. Chiacchiarini, C. De Angelo, Energy managment system designed for reducing operational costs of a hybrid fuel cell-battery-ultracapacitor vehicle, IEEE Vehicular Power and Propulsion Conference (IEEE VPPC 2020), Guijon, Spain. Nov. 18 to Dec. 16, 2020.

[6] Amaya, E. G., H. Chiacchiarini, C. De Angelo, and M. Asensio, “The energy management strategy of fc/battery vehicles winner of the 2017 IEEE VTS Motor Vehicles Challenge,” 2017 IEEE Vehicle Power and Propulsion Conference, VPPC 2017, pp. 1–6.

[7] Yue, M., S. Jemei, R. Gouriveau, and N. Zerhouni, "Review on health-conscious energy management strategies for fuel cell hybrid electric vehicles: Degradation models and strategies," Int. Journal of Hydrogen Energy, vol. 44, pp. 6844-6861, 2019.

[8] Utkin, V., Sliding modes in control and optimization, communication and control engineering. Berlin: Springer-Verlag, 1992.

[9] Song Z., Hou J., Hofmann H., Li J., Ouyang M., Sliding-mode and Lyapunov function-based control for battery/supercapacitor hybrid energy storage system used in electric vehicles, Energy, Vol. 122, 2017, Pages 601-612, ISSN 0360-5442.

[10] Wang B., Xu J., Xu D., Yan Z., Implementation of an estimator-based adaptive sliding mode control strategy for a boost converter based battery/supercapacitor hybrid energy storage system in electric vehicles, Energy Conversion and Management, Volume 151, 2017, Pages 562-572.

[11] Sira-Ramirez, Hebertt, Oliver-salazar, Marco, Vazquez-Santacruz, J.A. and Velasco-Villa, M.. (2011). On the robust control of the boost converter. 1497-1502. 10.1109/IECON.2011.6119529.

[12] Orozco E., and Chiacchiarini H. G, “Sliding mode control of a hybrid battery-supercapacitor energy management system” 2nd ASCENT conference, march 2021, Mexico.

[13] Orozco E. and Chiacchiarini H.G., Sliding Mode Control of a Hybrid Fuel Cell-Battery-Supercapacitor Energy Management System, XIX Reunión de Trabajo en Procesamiento de la Información y Control, San Juan, 2021

[14] Oldham, K. B. "A Gouy-Chapman-Stern model of the double layer at a (metal)/(ionic liquid) interface." J. Electroanalytical Chem. Vol. 613, No. 2, 2008, pp. 131–38.

[15] Xu, N., and J. Riley. "Nonlinear analysis of a classical system: The double-layer capacitor." Electrochemistry Communications. Vol. 13, No. 10, 2011, pp. 1077–81.

[16] Tremblay, O., L.-A. Dessaint, “Experimental validation of a battery dynamic model for ev applications.” World Electric Vehicle Journal. Vol. 3, May 13–16, 2009.

[17] Njoya, S. M., O. Tremblay, and L. -A. Dessaint. A generic fuel cell model for the simulation of fuel cell vehicles. Vehicle Power and Propulsion Conference, 2009, VPPC '09, IEEE. Sept. 7–10, 2009, pp. 1722–29.

[18] Motapon, S.N., O. Tremblay, and L. -A. Dessaint. "Development of a generic fuel cell model: application to a fuel cell vehicle simulation." Int. J. of Pow. Electronics. Vol. 4, No. 6, 2012, pp. 505–22.